Structural Engineering and Mechanics, *Vol. 55, No. 6 (2015) 1099-1120*
DOI: http://dx.doi.org/10.12989/sem.2015.55.6.1099

Behaviour of continuous prestressed concrete beams with external tendons

K.H. Enoch Chan*[1] and Francis T.K. Au[2a]

[1]*CH2M HILL, Burderop Park, Swindon, United Kingdom*
[2]*Department of Civil Engineering, The University of Hong Kong, Pokfulam, Hong Kong*

(Received October 14, 2014, Revised July 30, 2015, Accepted August 30, 2015)

Abstract. External prestressing has been applied to both new construction and retrofitting of existing reinforced and prestressed concrete structures. Continuous beams are preferred to simply supported beams because of economy, fewer movement joints and possible benefits from moment redistribution. However, this paper argues that continuous prestressed concrete beams with external unbonded tendons demonstrate different full-range behaviour compared to reinforced concrete (RC) beams. Applying the same design approach for RC to external prestressing may lead to design with a lower safety margin. To better understand the behaviour of continuous prestressed concrete beams with unbonded tendons, an experimental investigation is performed in which nine such specimens are tested to failure. The full-range behaviour is investigated with reference to moment-curvature relationship and moment redistribution. The amounts of moment redistribution measured in the experiments are compared with those allowed by BS 8110, EC2 and ACI 318. Design equations are also proposed to estimate the curvature ductility index of unbonded prestressed concrete beams.

Keywords: continuous beams; ductility; full-range behaviour; moment redistribution; partial prestressing; prestressed concrete; unbonded prestressing tendons

1. Introduction

External prestressing has been gaining popularity due to easy inspection, monitoring, restressing and replacement of tendons, and the potential corrosion risks with internal bonded tendons caused by incomplete penetration of grout. External prestressing avoids placing ducts within concrete, which facilitates steel fixing and use of thinner webs, thereby reducing the dead load. The applications of external unbonded prestressing can be found in construction of new structures and retrofitting, both in simply supported and continuous forms. In bridge construction, the continuous form is often preferred as it requires fewer movement joints, resulting in better riding quality and lower maintenance cost. Continuous beams also have higher stiffness than the corresponding simply supported beams. Continuous beams may be analysed by elastic theory with moment redistribution applied afterwards. This allows the designer to transfer bending moment

*Corresponding author, Chartered Bridge Engineer, E-mail: enoch.chan@ch2m.com
[a]Professor, E-mail: francis.au@hku.hk

http://www.techno-press.org/?journal=sem&subpage=8 ISSN: 1225-4568 (Print), 1598-6217 (Online)

from regions with congested reinforcement such as interior supports to less congested regions such as mid-span locations. The resulting reduction of reinforcement enables easier compaction of concrete and thus better concrete quality can be assured. When several load cases are considered, strategic use of moment redistribution reduces the peaks of bending moment envelope, and helps to achieve a more economical design.

Major design codes, such as BS 8110 (1997), EC2 (2004) and ACI 318 (2011), permit the use of linear elastic analysis with moment redistribution for the design of reinforced concrete (RC) and prestressed concrete (PC) beams. In BS 8110 and EC2, the degree of moment redistribution is expressed as $\beta=M_{\text{red}}/M_{\text{el}}$, where M_{el} is the bending moment obtained from linear analysis and M_{red} is that after redistribution. A value less than unity indicates that bending moment is redistributed away, and vice versa. The determination of β depends on the ductility of the critical sections. The relevant provisions in BS 8100, EC2 and ACI 318-11 are summarized below:

(a) BS 8110 expresses β as a function of x/d where x is the neutral axis depth and d is the effective depth, and the lower limit for β depends on the type of structure, namely

$$\beta \geq \frac{x}{d} + 0.4 \tag{1a}$$

$$\beta \geq \begin{cases} 0.7 & \text{for RC beams} \\ 0.8 & \text{for PC beams} \end{cases} \tag{1b}$$

(b) EC2 allows the use of linear elastic analysis with moment redistribution in continuous beams or slabs which are predominantly subjected to flexure and have a ratio of lengths of adjacent spans in the range 0.5 to 2. Apart from x/d, β also depends on concrete strength and the type of reinforcement, namely

$$\beta \geq \begin{cases} 0.44 + 1.25\left(0.6 + \dfrac{0.0014}{\varepsilon_{cu}}\right)\dfrac{x}{d} & \text{for } f_{ck} \leq 50 \text{ MPa} \\ 0.54 + 1.25\left(0.6 + \dfrac{0.0014}{\varepsilon_{cu}}\right)\dfrac{x}{d} & \text{for } f_{ck} > 50 \text{ MPa} \end{cases} \tag{2a}$$

$$\beta \geq \begin{cases} 0.7 & \text{for high - and normal - ductility steel} \\ 0.8 & \text{for low ductility steel} \end{cases} \tag{2b}$$

where ε_{cu} is the ultimate compressive strain in concrete and f_{ck} is the characteristic value of concrete cylinder compressive strength.

(c) ACI 318-11 controls by imposing limits on the net tensile strain in the extreme tension steel ε_t. Negative or hogging moments shall be redistributed when ε_t is 0.0075 or above at the section at which moment is reduced and such increase or decrease shall be no more than $1000\varepsilon_t$%, with a maximum of 20%.

As the flexural stiffness deviates from the original value due to concrete cracking and development of plastic hinges, the bending moments also change from the elastic bending moments. By definition, the flexural stiffness is the slope of moment-curvature relationship. RC and bonded PC sections therefore have almost zero stiffness after steel yielding since the moment is generally assumed to remain constant at the ultimate value (Fig. 1(a)). This idealised form has been adopted in several discussions regarding moment redistribution (Park and Paulay 1975, Wyche *et al.* 1992, Bondy 2003). However, for unbonded prestressed concrete (UPC), the

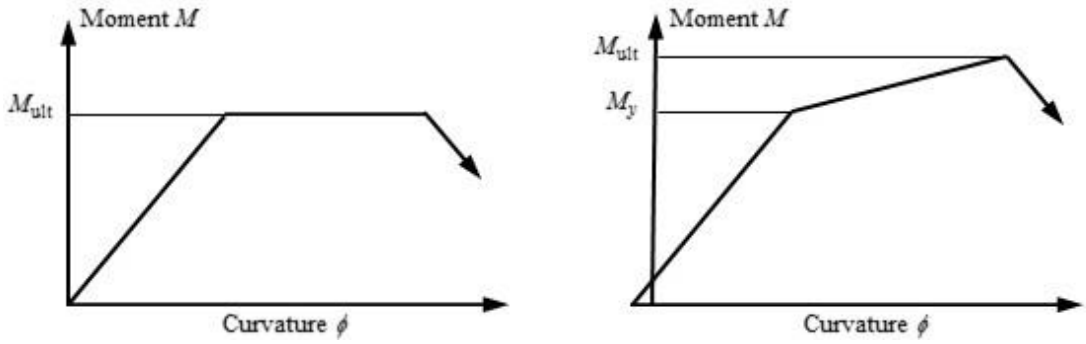

Fig. 1 Idealised moment-curvature relationship for (a) reinforced concrete beams and (b) unbonded prestressed concrete beams

moment-curvature relationship still exhibits an upward sloping branch after yielding of non-prestressed tension reinforcement until the peak moment is reached (Fig. 1(b)) because the tendons remain elastic throughout. This difference in moment-curvature relationship, especially the flexural stiffness after yielding of reinforcement, has a significant influence on moment redistribution and failure mode. Furthermore, the extent to which a section can undergo plastic deformation or the flexural ductility is generally less in a UPC beam section than in RC sections (Au *et al.* 2009). The current investigation will further look into the flexural ductility of continuous PC beams with external tendons. It is not the intention of this paper to compare the behaviour of UPC beam with RC beams, but to highlight the fact that the assumptions commonly adopted for RC beams may not be applicable to UPC.

2. Literature review

Many experimental and numerical investigations of unbonded prestressed concrete (UPC) members have been carried out in the past five decades. However, the previous studies were mainly concentrated on ultimate tendon stress at ultimate. Based on different parameters, such as loading type, span-depth ratio, concrete compressive strength, amounts of prestressing tendons and non-prestressed reinforcement, etc., several design formulae were proposed to estimate the tendon stress at ultimate. Comprehensive reviews of the state-of-the-art were reported by various researchers including Naaman and Alkhairi (1991), Allouche *et al.* (1998), Au and Du (2004). Various research groups have also extended their investigations to continuous PC members with external or internal unbonded tendons (Au and Du 2004, Allouche *et al.* 1999, Harajli *et al.* 2002).

Unlike simply supported beams, continuous beams undergo moment redistribution when there is a change in the relative flexural stiffness. Experiments have shown that UPC beams have substantial moment redistribution under loading. Aravinthan *et al.* (1995) carried out tests on two-span continuous PC beams with external tendons. One specimen was cast monolithically, while the other three were assembled segment by segment. The amount of confinement reinforcement at the potential plastic hinge regions was also varied in different specimens. Two-point loading was applied on each span and the applied load was symmetrical about the interior support. As the specimens were loaded to failure, interior support section had positive moment redistribution

ranging from 7.8% to 21.0%, with a larger amount of moment redistribution recorded for the specimen cast monolithically than the segmental one with the same degree of confinement. Aravinthan *et al*. (1996) continued the experimental programme while testing three externally prestressed precast segmental beams with unsymmetrical loading comprising two point loads on each span. Specimens, both with and without internal bonded tendons, demonstrated significant redistribution of moment. Test results show that moment redistribution at interior support section has negative moment redistribution from 47.8% to 61.5% for the case without internal bonded tendons. Aravinthan *et al.* (2005) further extended to continuous PC girders with highly eccentric external tendons. For specimens loaded on both spans, yielding of external tendons, which is not common in ordinary externally or unbonded prestressed concrete members, was observed. Aravinthan *et al.* (2005) concluded that the specimens with unsymmetrical loading demonstrated insignificant moment redistribution in contrast to a substantial amount as observed in a previous experiment (Aravinthan *et al.* 1996). Therefore PC beams with highly eccentric external tendons should be categorised as a special type with different structural behaviour.

Various researchers have developed numerical models for the analysis of PC members with external or unbonded internal tendons. They include the model composed of rigid bodies separated by cracks (Virlogeux 1988), models using incremental deformation method (Alkhairi and Naaman 1993, Harajli *et al.* 1999), models based on finite element methods (Jaiswal 2008, Du *et al.* 2008, Lou *et al.* 2013) and other methods (Wu and Lu 2003, Pisani 1996). According to the numerical analyses of flexural ductility of Au *et al.* (2009), UPC beams in general have lower flexural ductility than RC beams. This causes concern as the amount of moment redistribution depends on the flexural ductility of critical plastic hinge. Lou *et al.* (2013) proposed a numerical method to analyse two-span continuous prestressed concrete beams with internal unbonded tendons, and presented analysis results of three specimens with different non-prestressed steel. In particular, the paper has described the development of support reactions and bending moments of critical sections over the entire loading ranges of the three specimens. A more comprehensive study is necessary to understand the moment redistribution behaviour of continuous UPC beams.

3. Behaviour of continuous UPC beams

Tendons in UPC beams usually remain elastic up to failure of the members, which gives moment-curvature relationships different from those of RC beams. This becomes obvious after yielding of non-prestressed reinforcement, and hence UPC beams have much higher flexural stiffness than RC members in the pre-peak plastic region. To illustrate the effect of moment-curvature relationship on the full-range behaviour of a continuous beam, an RC beam and a UPC beam are studied. For simplicity, all sections are assumed to have the same moment-curvature relationship whether under sagging or hogging moment, and dead load is neglected.

Fig. 2(a) shows a continuous prismatic RC beam with two equal spans designed to carry two identical point loads at mid-span. When each point load reaches P_1, the section above the interior support reaches its ultimate moment capacity and develops a plastic hinge there (Fig. 2(b)). With further increase in loading, the plastic hinge above interior support rotates at a constant moment of resistance M_{ult} (Fig. 2(e)), while the mid-span sections take up the additional bending moment (Fig. 2(f)). The ability to take additional load depends on the flexural ductility of the plastic hinge as well as the ultimate moment capacity at the other sections, and thus there are two possible failure modes. Provided that the interior support section has sufficient ductility, the structure can

(a) Beam befor load is applied

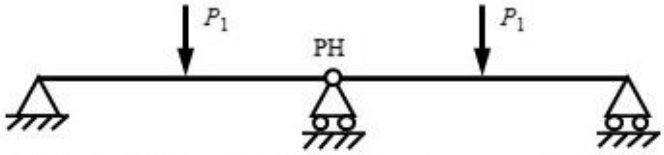

(b) A plastic hinge (PH) forms at interior support when load P_1 is applied on each span

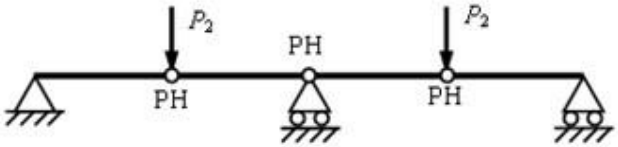

(c) Two more PHs form at mid-span under P_2 if section above interior support has adequate ductility

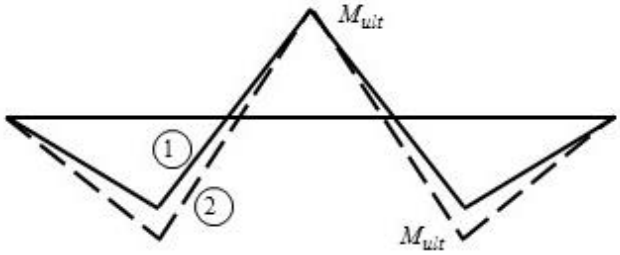

(d) Bending moment diagrams under P_1 and P_2

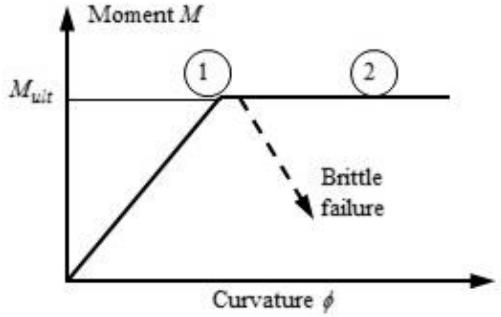

(e) Moment-curvature relationship at interior support

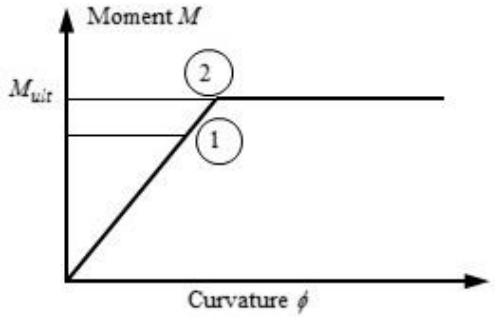

(f) Moment-curvature relationship at mid-span

Fig. 2 Schematic diagrams showing development of plastic hinges in a continuous reinforced concrete beam with two equal spans

take higher loading P_2 when the mid-span sections reach their ultimate moment capacities, forming additional plastic hinges and leading to beam collapse (Fig. 2(c)). If the interior support section does not have adequate flexural ductility, brittle flexural failure will occur there (Fig. 2(e)) before the mid-span sections reach their ultimate moment capacities. The bending moment diagrams for loading P_1 and P_2 shown in Fig. 2(d) indicate redistribution of bending moment from the interior support section to the mid-span sections.

(a) Unbonded prestressed concrete beam before load is applied

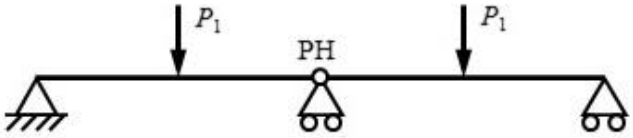

(b) A plastic hinge (PH) forms at interior support when load P_1 is applied on each span

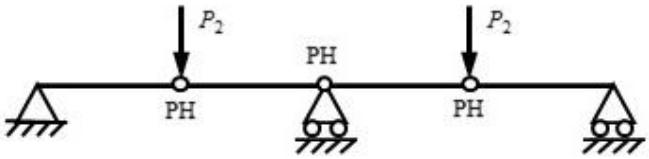

(c) Two more PHs form at mid-span under P_2 if section above interior support has adequate ductility

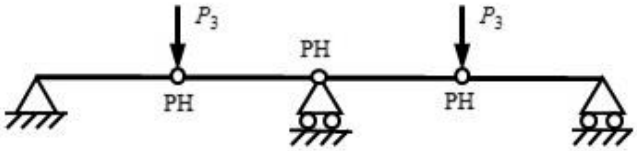

(d) The beam can support load up to P_3 when one of the plastic hinges has reached its ultimate rotational capacity

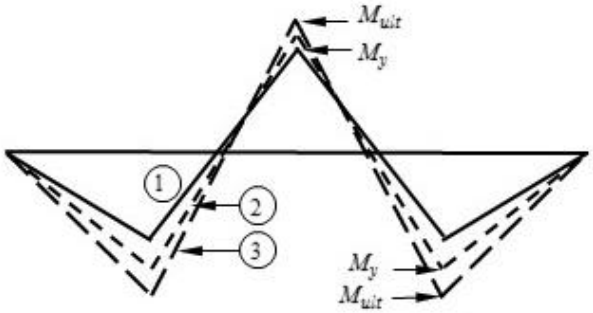

(e) Bending moment diagrams under P_1, P_2 and P_3

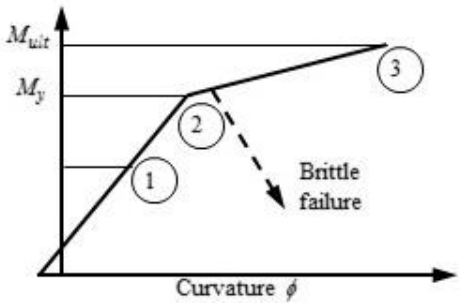

(f) Moment-curvature relationship at mid-span

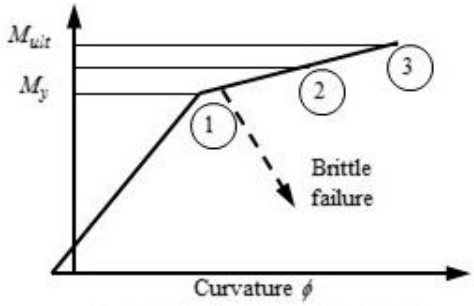

(g) Moment-curvature relationship at interior support

Fig. 3 Schematic diagrams showing the development of plastic hinges in an unbonded prestressed concrete beam with two equal spans

The prevailing prestress in the corresponding continuous UPC beam normally causes initial curvatures with camber in the spans before load application (Fig. 3(a)). For simplicity in illustration, the secondary moment is taken to be negligible or nil with the choice of a concordant profile. As before when each point load reaches P_1, the interior support section develops a plastic hinge (Fig. 3(b)). With further increase in loading, moment redistribution takes place due to reduction in flexural stiffness at interior support and the mid-span sections reach the yield moment when each point load increases to P_2 (Fig. 3(c)). However, unlike RC beams, it does not lead to immediate collapse. UPC beams can resist additional load even though plastic hinges form at the interior support and mid-span sections, because the flexural stiffness after yielding remains high in UPC beams (Figs. 3(f) and (g)). The beam eventually reaches its peak load P_3 when one of the plastic hinges fails (Fig. 3(d)). So far the interior support section is assumed to be ductile enough to satisfy the rotation demand. If the interior support section is brittle, the beam will collapse before plastic hinges are formed at the mid-span sections. Fig. 3(e) shows the bending moment diagrams for loading P_1, P_2 and P_3. The distribution of bending moment beyond plastic hinge formation at interior support and mid-span section is dependent on the relative sectional stiffnesses. The amount of moment redistribution is therefore a function of the flexural stiffness after steel yielding. It is obvious that the failure mechanism also depends on the load pattern. The sequence of plastic hinge formation may be different from those described above when the members are loaded unsymmetrically. This paper does not intent to extract all the possible scenarios, but to point out the unique characteristics of continuous UPC beams. Further investigation should be carried out to provide the complete picture.

The major differences between the general behaviour of RC and UPC beams upon being loaded to failure are summarised as follows:

(a) Since the moment-curvature relationship of RC beams is roughly elastic-perfectly plastic, a two-span RC beam collapses after formation of plastic hinges at the interior support and mid-span sections. In contrast, after the formation of 3 plastic hinges, the corresponding UPC beam can still support additional load because of the residual flexural stiffness after yielding of non-prestressed reinforcement.

(b) The failure of a two-span RC beam is governed by flexural strength and ductility at the interior support section but not by those at the mid-span sections because a mechanism results after formation of plastic hinges at mid-span sections. However for UPC beams, failure is governed by the flexural strength and ductility of interior support and mid-span sections. As failure occurs when one of the plastic hinges reaches its ultimate curvature, the mid-span sections should also be detailed with sufficient flexural ductility to avoid premature failure. Design codes BS 8110, EC2 and ACI 318 do not require the checking of ductility at mid-span sections in determining the degree of moment redistribution.

(c) In design to BS 8110, EC2 and ACI 318, moment is assumed to be redistributed from the first plastic hinge to the rest of the structure at the ultimate limit state. However, the actual "direction" of moment redistribution is not obvious for UPC beams, especially when the interior support and mid-span sections have yielded. The redistribution of bending moment depends on the relative flexural stiffness along the beam.

4. Experimental programme

This paper reports the results of 9 two-span continuous concrete beams partially prestressed

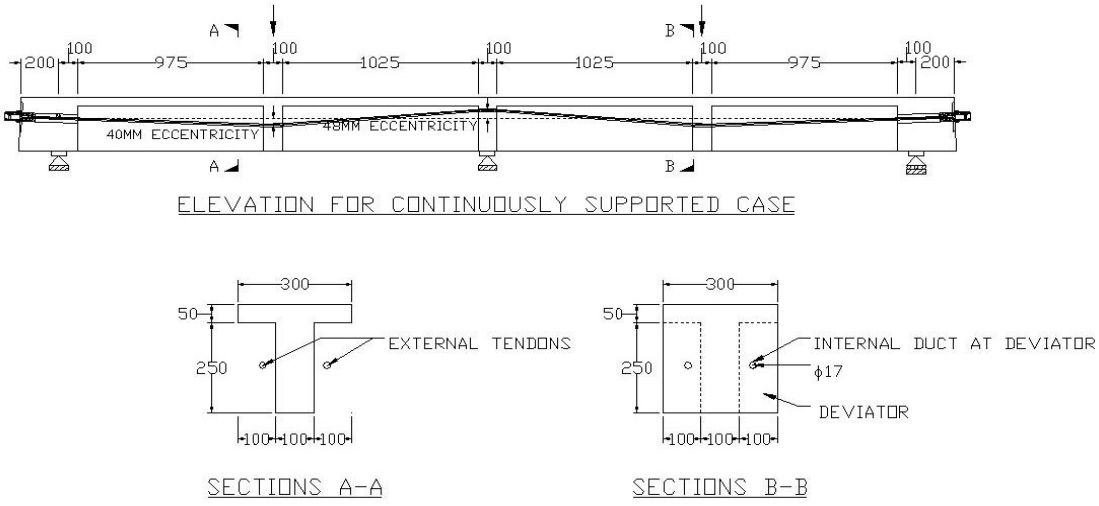

Fig. 4 Dimensions of test specimens

with external tendons, which are divided into two categories. Seven of them (SCS7 to SCS13) were prestressed before testing. To investigate the effect of prior loading history on the behaviour of RC beams strengthened with external tendons, the other two (SCS14 and SCS15) had been loaded before being prestressed with tendons. All specimens were eventually loaded to failure with large deflection so that the full-range behaviour could be investigated. To quantify the total amount of flexural reinforcement in a partial prestressing system, the reinforcement index ω can be used, namely

$$\omega = \frac{A_p f_{ps} + A_s f_s - A_s' f_s'}{bd f_c'} \tag{3}$$

where A_p is the cross sectional area of prestressing tendon, A_s and A_s' are the cross sectional areas of the bottom and top non-prestressed steel respectively, b is the width of the section, d is the depth to the centroid of tensile force, f_{ps} is the tendon stress at peak load, f_s and f_s' are the tensile stresses of the bottom and top non-prestressed steel at ultimate respectively, and f_c' is the in situ concrete compressive strength. Specimens with reinforcement indices at interior support ranging from 0.20 to 0.33 were tested. For specimens having the same amount of prestressed and non-prestressed reinforcement, different concrete strengths, namely grades 55, 70 and 100, were used to investigate the influence of concrete strength on the behaviour of PC beams with external tendons. Fig. 4 shows the dimensions of the test specimens while the properties of the specimens are shown in Tables 1 and 2.

All the specimens were post-tensioned with two external unbonded tendons in the morning of loading test. 7-wire steel strands of 12.9 mm nominal diameter were adopted and wedge-and-barrel systems were used as anchorages. The tendons were greased in the vicinity of the deviators and end blocks before tensioning in order to reduce friction. Both tendons were tensioned simultaneously using two identical hydraulic jacks connected to the same pump. Each tendon was installed with two load cells at the ends to monitor the variation of tendon force during post-tensioning and the subsequent loading test. Electrical foil strain gauges were also used to measure

Table 1 Prestressing and reinforcement details of test specimens

Specimen No.	SCS7	SCS8	SCS9	SCS10	SCS11	SCS12	SCS13	SCS14*	SCS15*
No.×Span (mm)	2×2250								
Tendon length L_t (mm)	4900								
Nominal concrete grade	70			100			55		
f_{cu} (MPa)	72	69	70	95	100	54	58	56	57
f_c' (MPa)	60	63	63	76	80	50	50	49	53
Reinforcement index ω									
at interior support	0.26	0.31	0.29	0.25	0.22	0.35	0.34	0.36	0.33
at mid-span	0.14	0.12	0.13	0.10	0.10	0.13	0.14	0.13	0.14
Top reinforcement	4T10								
A_s' (mm^2)	315	312	312	312	312	316	316	316	316
f_y' (MPa)	558	560	560	560	560	568	568	568	568
Bottom reinforcement	2T16	2T10	2T12	2T10	2T12	2T10	2T12	2T10	2T12
A_s (mm^2)	404	156	229	156	229	158	222	158	222
f_y (MPa)	554	560	590	560	590	568	556	568	556
Type of tendon	7-wire steel strands								
A_p (mm^2)	198								
f_{pe} (MPa)	1958								
Prestressing force (kN)	74.4	77.4	73.1	83.3	80.4	81.7	81.3	80.0	83.4
Prestressing level (%)	19.2	20.0	18.8	21.5	20.7	21.1	21.0	20.6	21.5
E_p (MPa)	201,900								
f_{py} (MPa)	1,819								
f_{pu} (MPa)	1,958								

* The specimens were pre-loaded to cracking before they were strengthened and tested to failure.

Table 2 Mix proportion in concrete for test specimens

Concrete	Proportion by weight					Superplasticizer
Grade	cement	10 mm aggregates	sand	condensed silica fume	water	(g/m^3)
55	0.51	1.0	1.0	-	0.24	1,360
70	0.58	1.0	1.0	-	0.21	2,670
100	0.52	1.0	0.79	0.03	0.17	6,310

the tendon strain between the deviators. When the required prestressing force was reached, the tendons were locked up by the anchorage system. The prestressing level is defined as the ratio of the effective prestress f_{pe} to the ultimate stress f_{pu} in the tendon. The prestressing levels in the specimens tested ranged from 18.8% to 21.5%. For clarity of test results, a concordant profile was adopted for the tendons, and no secondary moment would be induced.

Strains in the longitudinal non-prestressed steel were measured by electrical foil strain gauges bonded to reinforcing bars cast inside the beams. The method of installation of strain gauges,

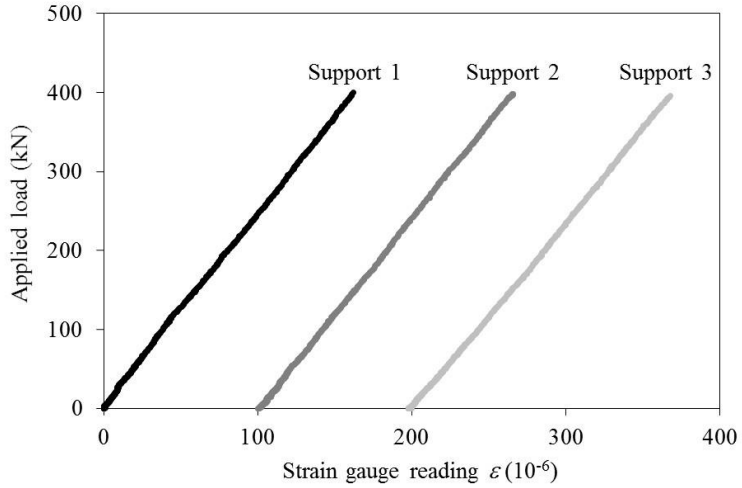

Fig. 5 Relationship between applied load and average strain increment at supports (graphs staggered for clarity)

which covers surface preparation, bonding and waterproofing, enables these gauges to cope with strains up to 3%. The vertical camber caused by post-tensioning and the subsequent vertical deflections during testing were measured with 22 linear variable displacement transducers (LVDTs). In addition, two LVDTs were installed at each end of the specimen to measure the horizontal displacements during testing. The LVDTs were zeroed before post-tensioning so that the effects of prestressing could also be picked up. The average curvature across a plastic hinge could also be picked up by the LVDTs.

Four strain gauges were installed on each support to measure the reaction. Calibration was carried out to correlate the average strain gauge reading with the vertical load applied on it of up to 400kN. The calibration graphs in Fig. 5 show that the support reactions could be measured with a satisfactory degree of accuracy using strain gauge readings. The bending moment diagram could then be constructed from the applied loading and support reactions.

A loading system comprising a hydraulic actuator and a steel loading beam was employed so that the specimen received two identical point loads above the mid-span deviators. Displacement control was adopted during loading in order to capture as much of the pre-peak and post-peak behaviour as possible. At each displacement increment during loading, vertical deflections, horizontal displacements at specimen ends, strains of non-prestressed steel and tendon forces were recorded.

5. Experimental results and discussion

5.1 General behaviour

One way of summarizing the behaviour of specimens during the loading tests is by plotting the applied moment against the curvature at critical sections. The moment-curvature relationships for all specimens are similar. Therefore Fig. 6 only presents the typical moment-curvature

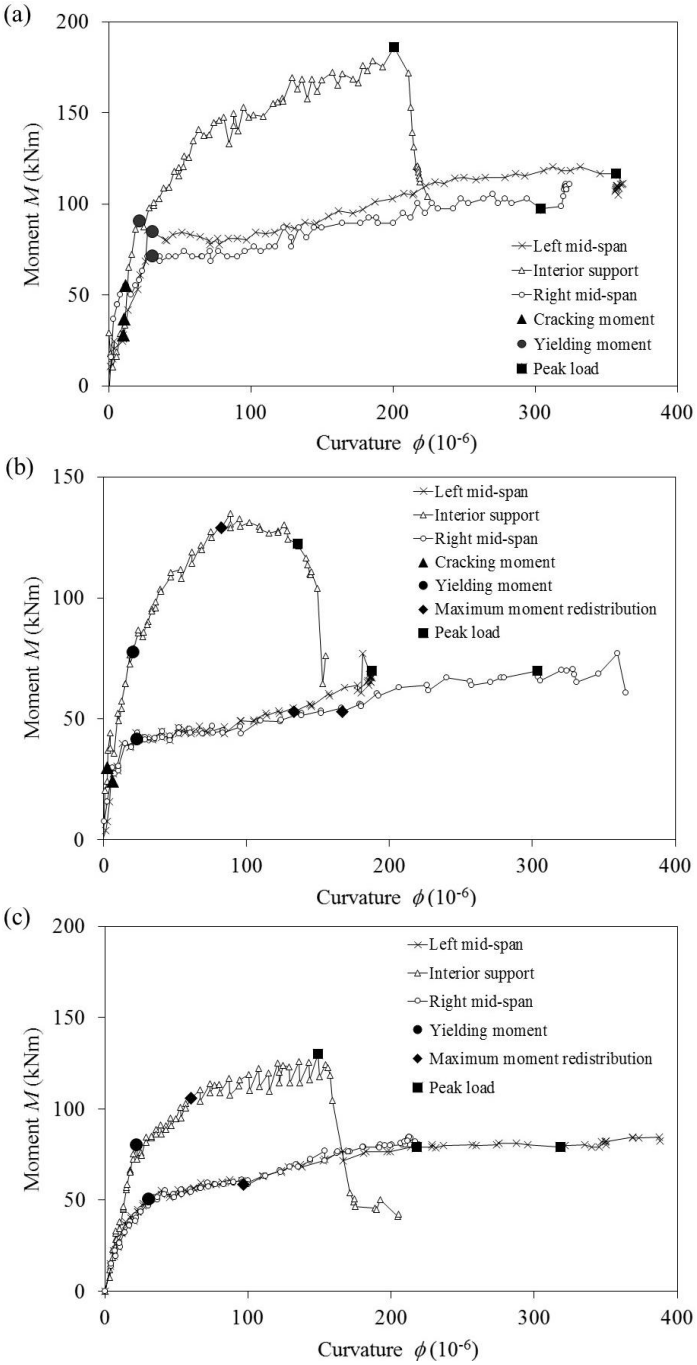

Fig. 6 Relationship between applied moment and curvature ϕ at interior support and mid-span for (a) SCS7, (b) SCS8 and (c) SCS15 after strengthening

relationships for critical sections of SCS7, SCS8 and SCS14. Markers to denote cracking and yielding moments, maximum moment redistribution and peak load have been included to assist

interpretation. Apart from SCS14 and SCS15 which have been pre-loaded to cracking before strengthening, all specimens follow a moment-curvature relationship with four distinct stages, namely (a) elastic, (b) cracked-elastic, (c) pre-peak plastic and (d) post-peak stage. The transition from the first to the second stage is caused by the development of cracks on the tension side of the beam, while the transition from the second to the third stage is caused by the yielding of non-prestressed steel. The end points of the first two stages, namely elastic and cracked-elastic respectively, can be identified as the first two kinks along each curve. The cracked-elastic stage is characterised by a reduction of stiffness compared to that of the elastic stage. The pre-peak plastic stage stretches from the yield point up to the peak load, which is relatively flat implying a reduced stiffness compared with the first two stages, while the post-peak stage is the subsequent portion. Before the peak load was reached, the beam deflection was roughly symmetrical about the interior support, as evidenced by the similar rates of progress along the moment-curvature relationship of the mid-span sections. This was however not the case after the concrete spalling around the interior support, which actually occurred on one side because of the stiffening effect of the tendon deviator. The span weakened by concrete spalling soon reached its maximum load capacity and entered the post-peak stage with decreasing load resistance, accompanied by further increase in curvature. The other span, however, remained robust and unloaded with reduction in curvature as the applied load decreased. As a result, there was reversal of curvature at one span while curvature increases at the other span.

Cracks began to appear at the second stage, and they continued to widen and propagate. In two-span continuous beams such as those tested, the largest moment often occurs at the interior support section as plastic hinges have not yet developed up to this stage and moment redistribution has not yet started. However, the maximum tensile stress may or may not be at the same section. The tensile stress under flexure also depends on the location of neutral axis which is a function of the section geometry, arrangement of steel reinforcement and prestressing force. This suggests that the first crack may appear at the interior support or mid-span section depending on various factors. For most of the specimens tested, cracking started at the top flange at the interior support. These cracks propagated downwards under a combination of flexural and shear stresses. Similar cracks were then formed at the bottom at mid-span sections and then propagated upwards. The cracks then propagated towards the centre of deviator at an inclined angle of 40° to 70° under the combined effect of flexure and shear. Except for SCS7 which eventually failed by shear, shear cracks were not detrimental to structural integrity since sufficient shear reinforcement was provided. New cracks were then opened up at fairly regular spacing and lengthened as the beam was being loaded. Upon the yielding of tension reinforcement, few or no more cracks were formed although the existing cracks kept on widening.

The specimens loaded to cracking before being strengthened by external prestressing, namely SCS14 and SCS15, displayed similar behaviour, except that the transitions from elastic to cracked-elastic stage was less obvious. In some cases, for example at the interior support section of SCS15, this transition no longer exists (Fig. 6(c)). On first loading to yielding, flexural and shear cracks appeared in a pattern similar to that in the other specimens. After strengthening by external prestressing followed by further application of loading, the original cracks simply re-opened under bending action. The effect of prior loading history on the load capacity can be investigated by comparing SCS14 with SCS12 and SCS15 with SCS13. In each pair of specimens, the same amount of non-prestressed reinforcement was provided and similar prestressing forces were applied. The peak loads are virtually the same for both specimens within the same group. For example, SCS12 and SCS14 have peak loads of 448kN and 448kN respectively, while the peak

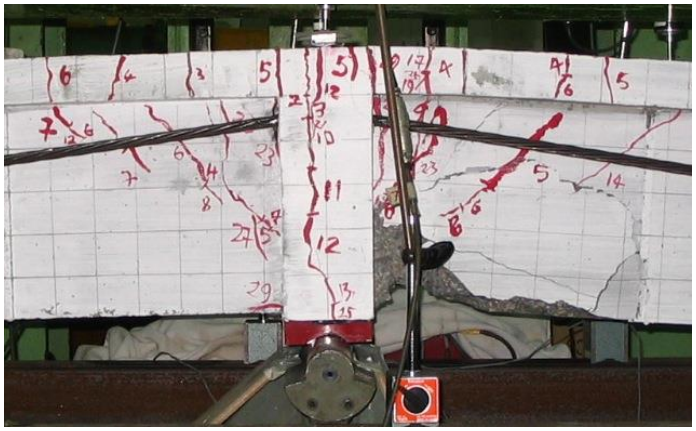

Fig. 7 Internal support region of Specimen SCS8 during test

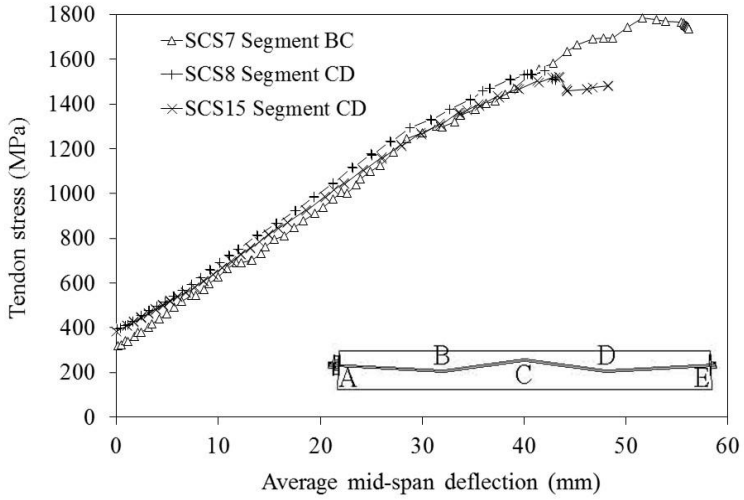

Fig. 8 Variation of tendon stress during loading test

loads of SCS13 and SCS15 are 522kN and 513kN respectively. This shows that prior loading history does not have significant effect on the peak load, even though the specimens have been loaded to yielding previously. Fig. 7 shows SCS8 during test.

The load cell readings and strain gauge readings for measurement of tendon forces all indicated that the tendons remained elastic throughout the loading process until the specimens failed, as shown in Fig. 8. Similar to the cases of simply supported beams (Au *et al.* 2008), the additional friction that occurred during the loading process was significant and the stresses shown in Fig. 8 were based on the parts with the highest cable forces.

One may understand the behaviour of UPC beams more by examining the moment-curvature curves in Fig. 6 in detail. The bending moment at a critical section is contributed to various extents by concrete compression, forces taken by top and bottom reinforcement, and tendon force. After reaching the yielding moments, all critical sections continued to increase in moment primarily due to the continuing increase in tendon force throughout the loading process. Most of the moments at

Table 3 Summary of test results

Specimen No.	SCS7	SCS8	SCS9	SCS10	SCS11	SCS12	SCS13	SCS14	SCS15
Reinforcement index									
at interior support	0.26	0.31	0.29	0.25	0.22	0.35	0.34	0.36	0.33
at mid-span	0.14	0.12	0.13	0.10	0.10	0.13	0.14	0.13	0.14
Cracking load (kN)	147	147	120	156	189	106	116.9	-*	-*
Yielding load (kN)	383	252	325	312	303	248	235	248	320
Peak load (kN)	675	463	556	491	556	447	522	448	513
Curvature ductility at interior support	9.6	6.8	6.5	7.4	11.0	5.5	8.3	6.4	7.0
Degree of moment redistribution at peak load									
at mid-span	0.84	0.87	0.80	0.71	0.59	0.75	0.92	0.85	0.76
at interior support	1.39	1.32	1.45	1.51	1.70	1.45	1.16	1.28	1.43

* The specimens were pre-loaded to cracking before they were strengthened and tested to failure.

critical sections continued increasing until the peak load was reached. In some cases such as SCS8, the moment at interior support section dropped gradually after reaching its maximum while the moments at mid-span sections continued increasing until the peak load was reached. After reaching the peak load, at least one of the critical sections experienced a drop in moment. Specimens that failed in flexure retained most of the strength after reaching the peak load until they reached the failure point characterized by an abrupt drop in resistance, which was triggered by concrete crushing and buckling of compression reinforcing bars at the critical section. On the other hand, shear failure as demonstrated in SCS7 was relatively brittle with a shorter post-peak range. Table 3 summarizes the test results obtained.

5.2 Reinforcement index and flexural ductility

Numerical investigations of bonded and unbonded PC beams have shown that the reinforcement index ω is a crucial parameter for describing flexural ductility since it is proportional to the neutral axis depth ratio x/d. Flexural ductility is the ability of a section to undergo plastic deformation. When a structure is designed for moment redistribution, the critical sections should be detailed with sufficient ductility. The curvature ductility factor μ_ϕ adopted here is defined in terms of the ultimate curvature ϕ_u and the curvature at first yield ϕ_y as

$$\mu_\phi = \frac{\phi_u}{\phi_y} \tag{4}$$

The ultimate curvature ϕ_u is taken as the curvature of the section when the resisting moment has dropped to 85% of the peak resisting moment after reaching the peak, while the yield curvature ϕ_y corresponds to that at the commencement of yielding. This definition as suggested by Park and Paulay (1975) gives a more reliable indication of how well a structure copes with overloading. In all of the specimens tested, the peak loads were governed by the smaller curvature ductility of plastic hinge in the vicinity of the interior support, as shown in Fig. 6. Both the reinforcement index ω and curvature ductility factor μ_ϕ are then computed for the plastic hinge next to the interior support in each of the test specimens under investigation and shown in Table 3.

In Table 3, the curvature ductility factors are based on the average curvature over the plastic hinge calculated from LVDT measurements rather than strain gauge measurements which are more affected by cracking in the vicinity. The relationship between reinforcement index and curvature ductility factor in Fig. 9 shows that curvature ductility decreases with increasing reinforcement index as expected. Moreover, for specimens with the same reinforcement index, specimens of higher concrete strength tend to be more brittle than those of lower concrete strength. Comparing the specimens which were pre-loaded to cracking before strengthening to those prestressed before loading, the ductility factors of the two groups agree reasonably well despite the highly uncertain nature of beam failure. Therefore prior loading history does not significantly affect the flexural ductility. Based on the experimental results, an equation for expressing the curvature ductility in terms of the reinforcement index is given as

$$\mu_\phi = \frac{1}{0.42\omega + 0.0094} \tag{5}$$

A lower-bound equation to provide a slightly conservative estimate of curvature ductility suitable for design purpose appears as

$$\mu_\phi = \frac{1}{0.42\omega + 0.038} \tag{6}$$

In BS 8110 and EC2, limits are imposed on x/d instead to ensure a minimum level of ductility. Therefore the curvature ductility factors are again plotted against the neutral axis depth ratio x/d at peak load. The average and lower-bound empirical equations in terms of x/d then appear as

$$\mu_\phi = \frac{1}{0.45(x/d) - 0.079} \quad \text{(Average)} \tag{7}$$

$$\mu_\phi = \frac{1}{0.45(x/d) - 0.05} \quad \text{(Lower bound)} \tag{8}$$

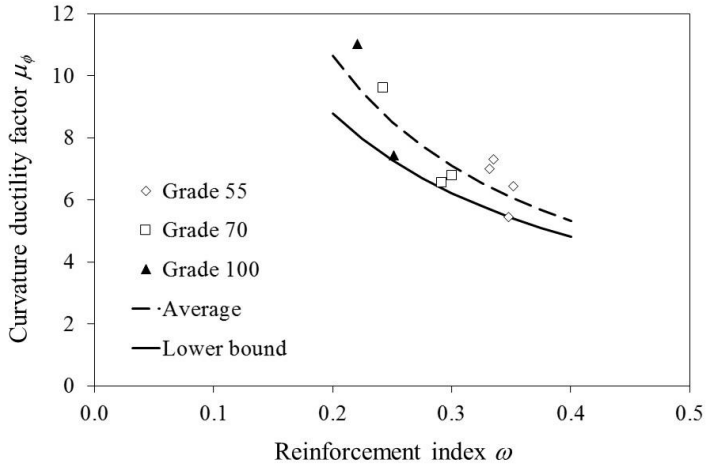

Fig. 9 Relationship between curvature ductility and reinforcement index

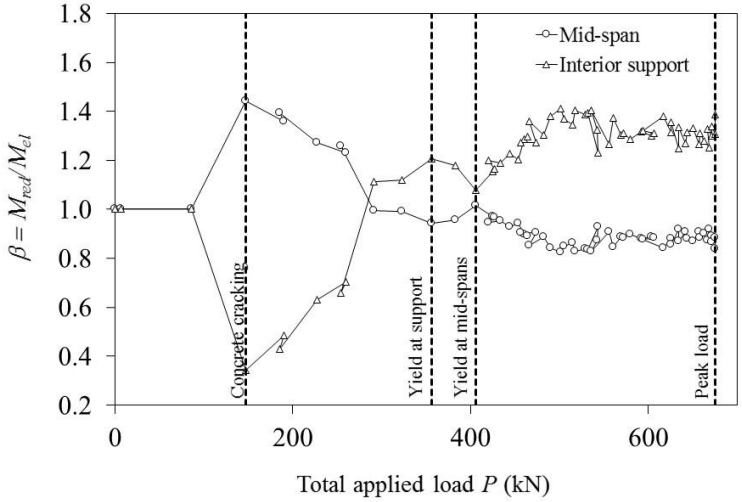

Fig. 10 Variation of moment redistribution in specimen SCS7

5.3 Moment redistribution

Fig. 10 shows the variation of degree of moment redistribution β for specimen SCS7 at different applied loads up to the peak. The non-prestressed tension reinforcement first yielded around the interior support, followed by the mid-span sections. In this case, collapse was due to shear failure in the vicinity of the interior support. Substantial moment redistribution resulting from concrete cracking was observed at a total applied load P of 147 kN. Moment redistribution at the elastic stage is often observed in RC beams and it is concluded that concrete cracking has a significant effect on moment redistribution (Scott and Whittle 2005). When the applied load exceeded 357 kN, the interior support section started to yield, leading to a decrease in the flexural stiffness there as shown in the moment-curvature plot (Fig. 6(a)). The change in flexural stiffness caused a reversal of β at interior support and mid-span sections. As the applied load kept increasing, the mid-span moments also increased (Fig. 11), eventually forming plastic hinges there. As a result, the flexural stiffnesses decreased locally at the mid-span sections, leading to another reversal of moment redistribution. Since then, the trend of β continued until collapse at P=675 kN with β=1.39 at interior support section and β=0.84 at mid-span sections. Although the first plastic hinge was formed around the interior support shedding moments elsewhere, bending moment was transferred back to the interior support section after the mid-span sections had yielded. Actually the hogging moment at the interior support section actually exceeded the elastic hogging moment at peak load. It is well-known that a change in the bending moment diagram due to moment redistribution also changes the shear force diagram. From equilibrium, the shear force just to the left of the interior support V_{int} can be expressed in terms of the bending moment at the interior support M_{int} as

$$V_{\text{int}} = \frac{2M_{\text{int}}}{L} + \frac{P}{4} \tag{9}$$

where L is the distance between end supports. Applying Eq. (9), the shear forces just next to the

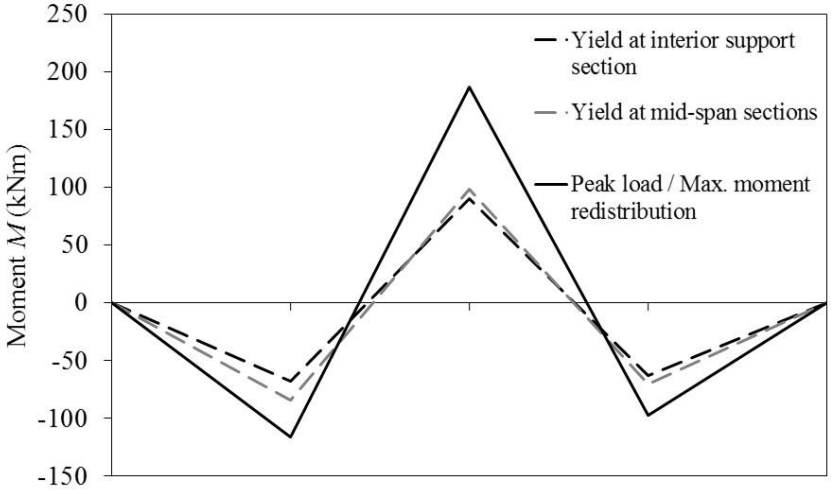

Fig. 11 Bending moment diagrams for specimen SCS7

interior support at peak load were calculated as 21% larger than that calculated from elastic analysis. The collapse due to shear failure near the interior support was to certain extent related to this.

Similarly the variation of degree of moment redistribution β for SCS8 is shown in Fig. 12. Actually except for SCS7 described above, yielding was observed at the mid-span sections before the interior support section for all other specimens including SCS8. All of them failed as the rotational capacity at the interior support section was reached. For SCS8, the sequence of plastic hinge formation is in a reversed order with plastic hinges formed first at mid-span sections at a total applied load of P=252 kN. Figs. 12 and 13 show that moment redistribution began at steel yielding at mid-span sections, leading to a larger bending moment at interior support section. The rate of development of moment redistribution slowed down after a plastic hinge was formed around the interior support section at P=294 kN. Nevertheless, the direction of moment redistribution did not reverse with bending moment still transferred from the spans to the interior support section until the degree of moment redistribution peaked at 1.53 with P=428 kN. At peak load of P=463 kN, the degree of moment redistribution β dropped to 1.32 around interior support section. The reversed trend of moment redistribution was due to concrete crushing and spalling around the interior support section at P=428 kN which also marked the maximum moment of resistance there. As P increased beyond 428 kN, bending moment decreased with increasing curvature, resulting in redistribution of bending moment away from the interior support section. Concrete crushing and spalling affected all other specimens except SCS7 which failed suddenly by shear before any signs of concrete crushing or spalling were observed. The effects on other specimens were similar but to different extent. Some resulted in a reversal of moment redistribution as in SCS8, while in other cases such as SCS11, the increase in degree of moment redistribution slowed down or halted as concrete crushing began. Such variations can be explained by the high degree of uncertainty and to certain extent randomness in the post-peak region.

The experimental programme shows that the general behaviour of UPC beams follows closely the qualitative analysis presented earlier based on a simplified moment-curvature relationship. UPC beams demonstrate fairly high flexural stiffness after yielding, especially at the interior

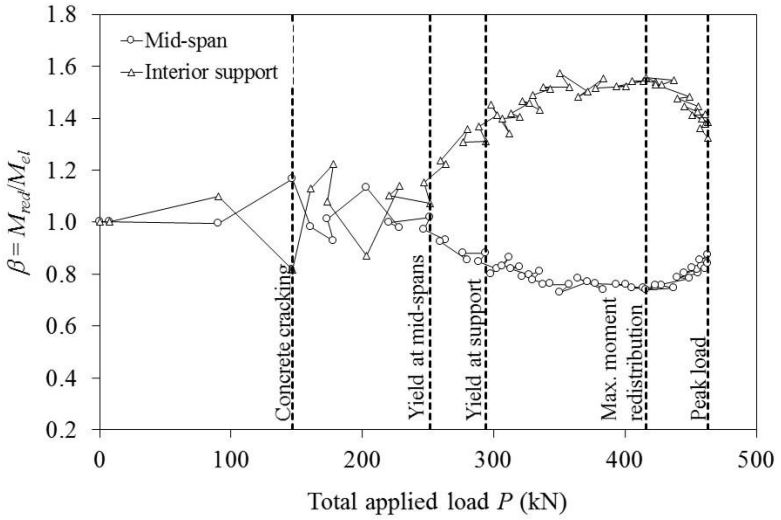

Fig. 12 Variation of moment redistribution in specimen SCS8

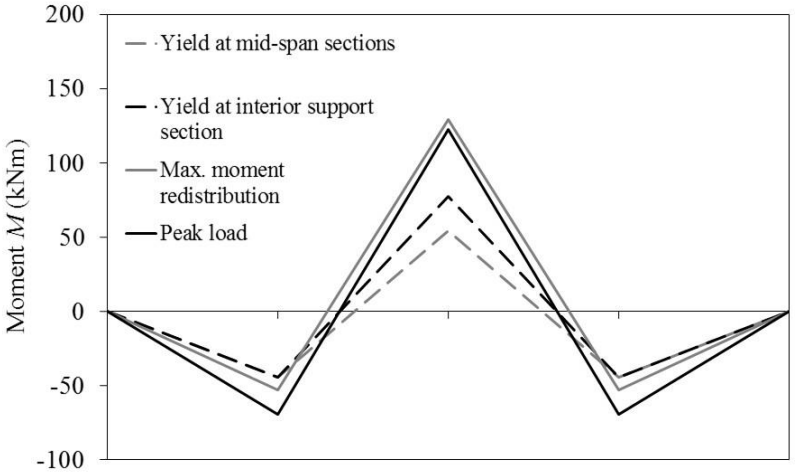

Fig. 13 Bending moment diagrams for specimen SCS8

support sections with higher reinforcement indices than those at the mid-span sections. They can resist substantial additional load after formation of plastic hinges at the interior support and mid-span sections. Although the location of first plastic hinge may be different as for example in SCS7 and SCS8, the failure is still initiated by that at the interior support section. Therefore the beam failure is governed by the least ductile section rather than the first plastic hinge assumed in BS 8110, EC2 and ACI 318. Investigation into the experimental results also agrees with an earlier conclusion that the direction of moment redistribution is not obvious for UPC beams, especially at peak load as the flexural stiffness is usually complicated by concrete crushing and spalling as well as buckling of steel reinforcement. Although beam design carried out according to BS 8110, EC2 and ACI 318 normally assumes the direction of moment redistribution to depend on one plastic

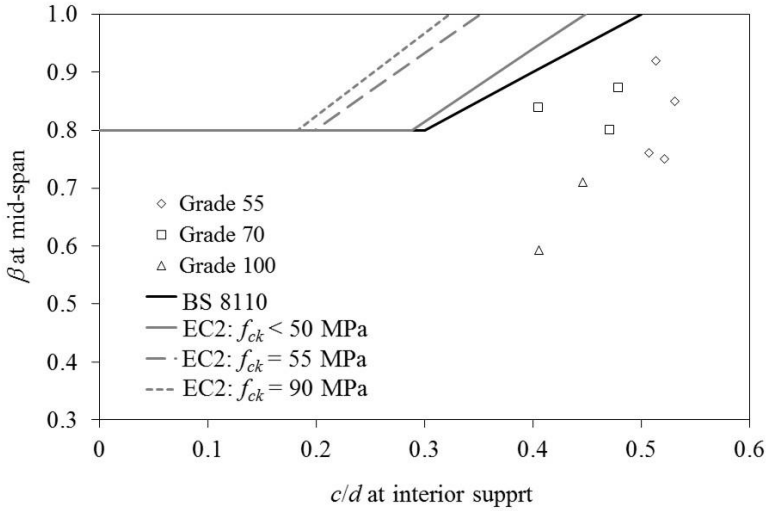

(a) Interior support section

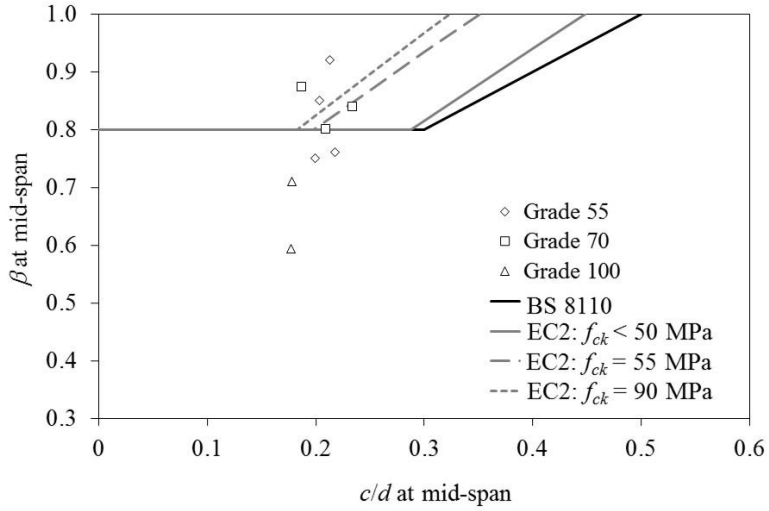

(b) Mid-span section

Fig. 14 Relationship between the degree of moment redistribution β and x/d ratio

hinge only, experimental results show that all critical sections play their roles in UPC beams. Last but not least, due to moment redistribution, the actual shear forces may deviate substantially from the shear forces calculated from elastic analysis. Such variations in shear force should be taken into account during the design process. Adopting the capacity design for shear (Park and Paulay 1975) in this case should be able to avoid such brittle shear failures.

Fig. 14 shows the relationship between the degree of moment redistribution β at peak load and neutral axis depth ratio x/d, plotted against the allowable moment redistribution according to BS 8110 and EC2. Neither the x/d ratio at interior support section nor that at mid-span section is adequate in describing the trend of β, because moment redistribution is primarily governed by the

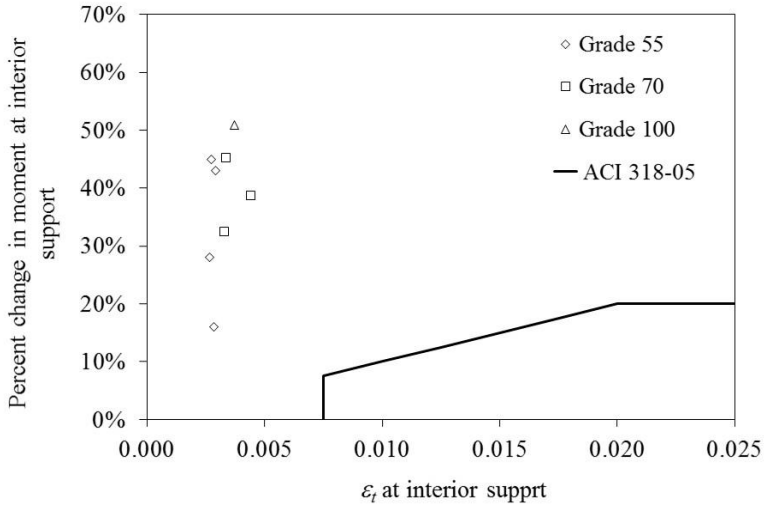

(a) Interior support section

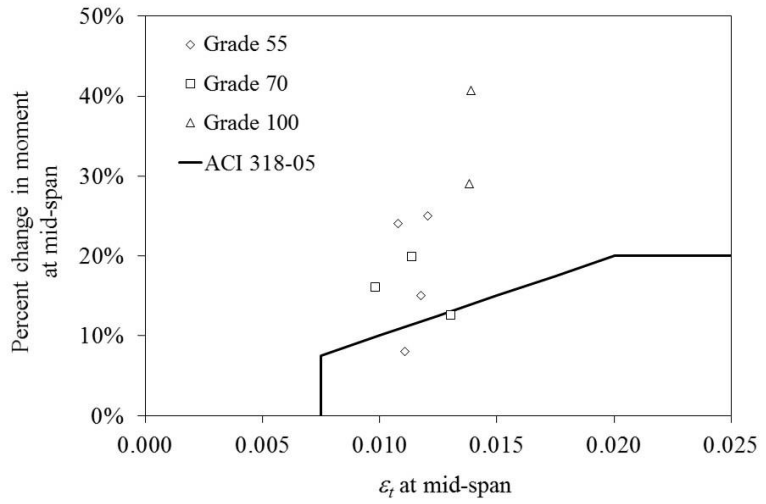

(b) Mid-span section

Fig. 15 Relationship between change in moment and net tensile strain in extreme tension steel ε_t

relative stiffnesses of various sections along the member. In other words, moment redistribution in UPC beams is member-dependent and each of the critical sections has a role to play. Since x/d is a property of a particular section or plastic hinge, it does not correlate well with the degree of moment redistribution. The allowable values of moment redistribution according to BS 8110 and EC2 primarily depend on x/d although the latter also takes into account the concrete strength. If the allowable moment redistribution is based on the x/d ratio at interior support section, the codes gives β on the safe side (Fig. 14(a)). However, if β is evaluated from the x/d ratio at mid-span section, β is unsafe in some cases (Fig. 14(b)). Incidentally, the specimens made of grade 100 concrete have the largest amount of moment redistribution among those tested. The effect of prior loading history on moment redistribution is insignificant.

The relative changes in moment, i.e., $|1-\beta|$, obtained from the experimental results are also plotted in Fig. 15 against the net tensile strain in the extreme tension steel ε_t and compared with the allowable values specified by ACI 318-11. As moment redistribution in UPC beams is primarily member-dependent, the correlation between the changes in moment and ε_t at a section is not strong as expected. It is however observed that the allowable values of moment redistribution specified by ACI 318-11 are mostly conservative in both types of section. To facilitate a complete understanding of the behaviour of continuous UPC structures, extensive parametric studies should be performed, and this is best carried out using a numerical model. However, from the experimental results obtained thus far, a more conservative degree of moment redistribution β should be adopted for continuous UPC beams in BS 8110 and EC2.

6. Conclusions

From results obtained from the experimental programme on UPC beams, the following conclusions are drawn.

(a) While an RC beam section has negligible flexural stiffness after steel yielding, the residual stiffness of a continuous UPC beam after formation of plastic hinges at interior support and mid-span sections is still substantial as the tendons normally remain elastic throughout.

(b) The ultimate failure of a continuous UPC beam is normally triggered by one of the plastic hinges reaching its ultimate curvature.

(c) In design of RC beams, existing design codes usually assume that the bending moment is redistributed away from the section where the first plastic hinge forms. However for UPC beams, the direction of moment redistribution at peak load is not obvious since plastic hinges may have formed at both the interior support and mid-span sections at peak load.

(d) The curvature ductility factor μ_ϕ at the critical section of UPC beams decreases with increasing reinforcement index ω or x/d ratio. For a constant ω or x/d ratio, μ_ϕ decreases with increasing concrete strength. Empirical equations have been obtained for estimation.

(e) The amount of moment redistribution at peak load does not have a clear trend with the x/d ratio at the interior support or mid-span section, nor with the net tensile strain in the extreme tension steel. This is because moment redistribution of a UPC beam is member-dependent since each of the plastic hinges along the beam plays a role.

Acknowledgments

The work described in this paper has been supported by the Research Grants Council of the Hong Kong Special Administrative Region, China (RGC Project No. HKU 7101/04E).

References

ACI Committee 318 (2011), *Building Code Requirements for Structural Concrete (ACI 318-11) and Commentary (ACI 318R-11)*, American Concrete Institute, Farmington Hills, MI, USA.

Alkhairi, F.M. and Naaman, A.E. (1993), "Analysis of beams prestressed with unbonded internal or external tendons", *ASCE J. Struct. Eng.*, **119**(9), 2680-2700.

Allouche, E.N., Campbell, T.I., Green, M.F. and Soudki, K.A. (1998), "Tendon stress in continuous unbonded prestressed concrete members-Part 1: review of literature", *PCI J.*, **43**(6), 86-93.
Allouche, E.N., Campbell, T.I., Green, M.F. and Soudki, K.A. (1999), "Tendon stress in continuous unbonded prestressed concrete members-Part 2: parametric study". *PCI J.*, **44**(1), 60-71.
Aravinthan, T., Mutsuyoshi, H., Fujioka, A. and Hishiki, Y. (1996), "Flexural behavior of two span continuous segmental PC beams with external tendons", *Tran. JPN Concrete Inst.*, **18**, 229-234.
Aravinthan, T., Mutsuyoshi, H., Matupayont, S. and Machida, A. (1995), "Moment redistribution in prestressed concrete continuous beams with external tendons", *Tran. JPN Concrete Inst.*, **17**, 197-202.
Aravinthan, T., Witchukreangkrai, E. and Mutsuyoshi, H. (2005), "Flexural behavior of two-span continuous prestressed concrete girders with highly eccentric external tendons", *ACI Struct. J.*, **102**(3), 402-411.
Au, F.T.K., Chan, K.H.E., Kwan, A.K.H. and Du, J.S. (2009), "Flexural ductility of prestressed concrete beams with unbonded tendons", *Comput. Concrete*, **6**(6), 451-472.
Au, F.T.K. and Du, J.S. (2004), "Prediction of ultimate stress in unbonded prestressed tendons", *Mag. Concrete Res.*, **56**(1), 1-11.
Au, F.T.K., Su, R.K.L., Tso, K. and Chan, K.H.E. (2008), "Behaviour of partially prestressed beams with external tendons", *Mag. Concrete Res.*, **60**(6), 455-467.
Bondy, K.B. (2003), "Moment redistribution: principles and practice using ACI 318-02", *PTI J.*, **1**(1), 3-21.
British Standards Institution (1997), BS 8110: Part 1: Structural Use of Concrete: Code of Practice for Design and Construction, BSI, London, UK.
European Committee for Standardisation (2004), Eurocode 2: Design of Concrete Structures-Part 1-1: General Rules and Rules for Buildings, European Committee for Standardisation, Brussels, Belgium.
Harajli, M.H., Khairallah, N. and Nassif, H. (1999), "Externally prestressed members: evaluation of second-order effects", *ASCE J. Struct. Eng.*, **125**(10), 1151-1161.
Harajli, M.H., Mabsout, M.E. and Al-hajj, J.A. (2002), "Response of externally post-tensioned continuous members", *ACI Struct. J.*, **99**(5), 671-680.
Jaiswal, O. (2008), "Effect of prestressing on the first flexural natural frequency of beams", *Struct. Eng. Mech.*, **28**(5), 515-524.
Du, J.S., Au, F.T.K., Cheung, Y.K. and Kwan, A.K.H. (2008), "Ductility analysis of prestressed concrete beams with unbounded tendons", *Eng. Struct.*, **30**(1), 13-21.
Lou, T., Lopes, S.M.R. and Lopes, A.V. (2013), "Nolinear and time-dependent analysis of continuous unbonded pretressed concrete beams", *Comput. Struct.*, **119**, 166-176.
Lou, T. and Xiang, Y. (2010), "Numerical analysis of second-order effects of externally prestressed concrete beams", *Struct. Eng. Mech.*, **35**(5), 631-643.
Naaman, A.E. and Alkhairi, F.M. (1991), "Stress at unbonded post-tensioned tendons: Part 1-evaluation of the state-of-the-art", *ACI Struct. J.*, **88**(5), 641-651.
Park, R. and Paulay, T. (1975), *Reinforced Concrete Structures*, John Wiley & Sons, New York, NY, USA.
Pisani, M.A. (1996), "A numerical model for externally prestressed beams", *Struct. Eng. Mech.*, **4**(2), 177-190.
Scott, R.H. and Whittle, RT. (2005), "Moment redistribution effects in beams", *Mag. Concrete Res.*, **57**(1), 9-20.
Virlogeux, M. (1988), "Nonlinear analysis of externally prestressed structures", *FIP Symposium Proceedings*, Jerusalem, Israel,.
Wu, X.H. and Lu, X.L. (2003), "Tendon model for nonlinear analysis of externally prestressed concrete structures", *ASCE J. Struct. Eng.*, **129**(1), 96-104.
Wyche, P.J., Uren, J.G. and Reynolds, G.C. (1992), "Interaction between prestress secondary moments, moment redistribution, and ductility-a treatise on the Australian concrete codes", *ACI Struct. J.*, **89**(1), 57-70.